TURBULENT PIPE FLOW CHARACTERISTICS OF LOW MOLECULAR WEIGHT POLYMER SOLUTIONS

A. Sá Pereira
Departamento de Engenharia Química, Instituto Superior de Engenharia do Porto
Rua de S.Tomé, 4200 Porto CODEX, Portugal

F. T. Pinho *
Departamento de Engenharia Mecânica e Gestão Industrial
Faculdade de Engenharia, Rua dos Bragas, 4099 Porto CODEX, Portugal

Abstract

Detailed mean velocity, normal Reynolds stress and pressure drop measurements were carried out with 0.4 to 0.6% by weight aqueous solutions of Tylose, a methylhydroxil cellulose of molecular weight equal to 6,000 from Hoechst after a selection process from a set of low molecular weight fluids. The viscosity measurements of the Tylose solutions showed shear-thinning behaviour, and the oscillatory and creep tests measured elastic components of the stress of the order of the minimum detectable values by the rheometer.

These low molecular weight polymer solutions delayed transition from the laminar to the turbulent regime and showed drag reductions of half that reported to occur with other low elasticity shear-thinning high molecular weight aqueous polymer solutions. Near the wall the axial turbulent stress was higher than with water, whereas the two transverse components of turbulence were reduced. This near-wall behaviour is typical of drag reducing fluids based on high molecular weight polymers, but in the core of the pipe the three components of turbulence were higher than for the water flows, especially in the radial and tangential directions.

1- Introduction

Various industrial processes involve the flow of non-Newtonian fluids under turbulent regime conditions. The understanding and optimization of these processes requires the previous knowledge and understanding of simpler and more fundamental flows, such as wall dominated flows. The great variety of non-Newtonian fluids also implies that such investigation must encompass fluids with very different rheological properties.

* Corresponding author

Seminal work on non-Newtonian pipe flow were those of Metzner and Reed [1] and Dodge and Metzner [2] who reported the variation of friction factor with Reynolds number in laminar, transitional and turbulent flows of shear-thinning fluids. Toms' [3] discovery of a reduction in the skin-friction coefficient in pipe flows in the late forties, and in other wall-dominated flows, such as in a square duct by Logan [4] and in channel flow by Donohue *et al* [5], promoted a wealth of research in the last 30 years in an effort to understand the relation between turbulence production/dissipation mechanisms and the observed drag reduction. In the late sixties dilute polymer flows had been thoroughly investigated in terms of pressure drop and mean velocity field and the phenomena of drag reduction reported to occur with a wide class of high molecular weight polymers ($> 10^5$) at very dilute concentrations. As a corolary to this extensive research Virk *et al* [6,7] derived empirical envelopes of maximum drag reduction for pressure and velocity and formulated a three-layer velocity model in wall coordinates.

Detailed mean and turbulent velocity measurements with very dilute aqueous solutions of heavy polymers ($M > 10^5$) were carried out by Reischmann and Tiederman [8], Achia and Thompson [9] and Allan *et al* [10] amongst others, who reported higher axial turbulence close to the wall and lower radial turbulence than with the solvent flows at the same Reynolds numbers. More recently, Tiederman *et al* [11] and Luchik and Tiederman [12] observed that these tendencies were associated with the damping of small eddies in the buffer layer and an increase in the average time between bursts from the wall region into the core of the flow.

These investigations were usually carried out with polymers of molecular weight between 10^5 and 6×10^6 and at very dilute concentrations, so that the shear viscosity remained constant and almost equal to the solvent viscosity. Another direction of research has been the investigation of the turbulent pipe flow characteristics of variable viscosity fluids (Shaver and Merril [13]) in the attempt to understand the behaviour of inelastic fluids. So far this quest has been somewhat confusing and elusive, because sometimes the same fluid has been reported as being elastic and inelastic by various authors. The typical case are the solutions of Carbopol which have been declared as elastic, inelastic and elastic but non-drag-reducer by Metzner and Park [14], Hartnett [15] and Edwards and Smith [16], respectively. Anyway, most of the times the strongest influence on the flow behaviour has been associated with elasticity.

The importance of such applications as oil drilling operations and waste water sludge flows has also promoted detailed research on viscoplastic turbulent pipe flows of Herschel-Bulkley fluids by Park *et al* [17] and Escudier *et al* [18], but this area still needs further work.

The recent investigations of Pinho and Whitelaw [19], and Escudier *et al* [18] of turbulent flows with shear-thinning polymer solutions with viscosity power law indices between 0.39 and 0.90 also showed drag reduction and the validity of Virk's asymptote for these variable viscosity fluids. The drag reduction was accompanied by a damping in both transverse turbulent quantities and a higher axial turbulence close to the wall. Berman [20] investigated the effect of molecular weight on drag reduction, but even its lower molecular weight polymer had a value of 2×10^5, and he concluded that the friction factor reduction increased with molecular weight.

Drag reduction has promoted the use of polymeric additives in industry whenever an increase in flow rate is required, such as during maintenance of pumping equipment in pipelines (Burger *et al* [21]). The use of polymer additives to reduce drag, and consequently pumping costs, has to be carefully balanced with its degradation rate and the consequent rate of polymer renewal, the investment on injection mechanisms and quantity of polymer necessary to achieve a certain drag reduction intensity, which may preclude its use in normal operating conditions, but not in special occasions such as maintenance of equipment. In this context, although long molecules are more efficient drag reducers than lighters molecules, their faster rate of degradation may suppress that advantage.

Drag reduction in turbulent pipe flows is a manifestation of elasticity, and according to Hinch [22], Tabor *et al* [23] and other workers, this is related to a strong strain imposed elongation of the molecules and its effect on viscosity, and therefore it is logic to expect that small light molecules may be inelastic and will show no drag reduction. This idea has been partially contradicted by the experiments of Lodes and Macho [24] with aqueous solutions of a 19,000 kg/kmole partially saponificated polyvinylacetate with different degrees of hydrolysis, which exhibited drag reductions close to the maximum predicted by Virk's asymptote (Virk *et al* [7]), but the authors failed to report any turbulence field data, and speculated on a different origin for the elastic behaviour of the fluid without proper evidence. It is clear that more information regarding the hydrodynamic behaviour of low molecular weight polymer solutions is necessary, especially regarding molecules which are at least one order of magnitude lighter than the majority of the fluids repeated in the past.

The objective of this work is the characterisation of the hydrodynamics of turbulent pipe flows of very low molecular weight polymer solutions of variable viscosity. This task is preceeded by the selection of an appropriate fluid from a set of low molecular weight polymers, and the investigation of its rheology in order to ascertain its viscous and possible elastic characteristics. The polymers under scrutiny in this work are three

times lighter than those of Lodes and Macho and more than one order of magnitude lighter than those used in the other above mentioned literature.

The next section describes the experimental methods and the uncertainties of the rheological and hydrodynamic measurements, and is followed by the presentation and discussion of the results. The paper ends with a summary of the main findings.

2 - Experimental Methods and Uncertainties

The hydrodynamic flow measurements were preceeded by the selection of an appropriate additive from a set of low molecular weight polymers according to optical, rheological and fluid dynamics criteria. Therefore, the description of the experimental equipment is divided into two sections: rheological equipment, and flow configuration and its instrumentation.

2.1 - Rheological Equipment

The rheological characterisation of the fluids was carried out in a rheometer from Physica, model Rheolab MC 100, made up of an universal measurement unit UM/MC fitted with a low viscosity double-gap concentric cylinder system. This geometry allowed the measurement of viscosities between 1 mPa.s and 67.4 mPas at the maximum shear rate of 4031 s^{-1}, and for higher viscosities a cone-plate system could also be mounted on the universal unit. The rheometer could be both stress and shear rate controlled, a possibility that was used according to the ranges of viscosity and shear rate under observation. A thermostatic bath and temperature control system, Viscotherm VT, allowed the control of temperature of the fluid sample within 0.1°C.

The rheometer was operated in steady state to measure the viscometric viscosity, in oscillatory flow to measure the elastic and viscous components of the dynamic viscosity, and creep tests were also carried out in an attempt to quantify the fluid elasticity in the wider possible manner. In the viscometric viscosity runs with the double gap concentric cylinder at low shear rates, the rheometer was operated in the controlled shear stress mode, and the uncertainty of the measurements was better than 3.5%, whereas at higher shear rates the shear rate control mode was used and the uncertainty was better than 2%. For shear rates above 1000 s^{-1} measurements of viscosity were also carried out with the cone-plate system in order to widen the measuring range up to a maximum shear rate of 5230 s^{-1}. The precision of this rheometer in the oscillatory tests was better than 10% with the low viscosity fluids under investigation, for frequencies of oscillation between 1 and 50 Hz. For the creep tests the uncertainty was better than 5% and 10% for high and low shear stresses, respectively.

2.2 - Flow Configuration and Instrumentation

The flow configuration is similar to that of Pinho and Whitelaw [19] and consisted of a long 26 mm inside diameter vertical pipe with a square outer cross section to reduce diffraction of light beams. The fluid circulated in a closed circuit, pumped from a 100 litre tank through 90 diameters of pipe to the transparent acrylic test section of 232 mm of length, and a further 27 diameters down back to the tank, with the flow controlled by two valves. A 100 mm long honeycomb was located 90 diameters upstream of the test section to help to ensure a fully developed flow in the plane of the measurements. This development length proved enough as can be confirmed in the water velocity measurements presented elsewhere (Pereira [25]), according to White [26] and the non-Newtonian measurements of Pinho and Whitelaw [19]. Four pressure taps 65 mm apart were drilled in the test section and the upstream pipe and were used for the pressure loss measurements. These pressure measurements also confirmed the fully developed flow situation in the test section.

Equal longitudinal pressure gradients were measured between any two consecutive taps, thus ensuring that the connection between the brass pipe and the test section was well done and within the machining tolerances of ± 10 μm, and caused no detectable harm to the flow condition.

The pressure drop was measured by means of a differential pressure transducer from Rosemount, model 1151 DP 3S which had a variable gain up to a maximum of 7.47 kPa. The transducer was fixed to the wall to avoid any movement and/or positioning effects on the calibration, and its output was sent to a computer via a data acquisition board Metrabyte DAS-8 interfaced with a Metrabyte ISO 4 multiplexer, both from Keithley. The calibration of the transducer was carried out in a special device made up of two independent water columns (Pereira [25]) with the water level checked by two precision rules with an accuracy better than 0.1 mm, so that the overall uncertainty of the pressure measurements was less than 1.2 Pa, which is about 1.6% and 5% for high and low pressure differences, respectively.

A fiber optic laser-Doppler velocimeter from INVENT, model DFLDA was used for the velocity measurements with a 30 mm probe mounted on the optical unit. Scattered light was collected by a photodiode in the forward scatter mode, and the main characteristics of the anemometer are listed in table I and described by Stieglmeier and Tropea [27]. The signal was processed by a TSI 1990C counter interfaced with a computer via a DOSTEK 1400 A card, which provided the statistical quantities. The data presented in this paper has been corrected for the effects of the mean gradient broadening and the maximum uncertainties in the axial mean and rms velocities at a

95% confidence level are of 2% and 3.1% on axis respectively, and of 2.8% and 7.1% in the wall region. The maximum uncertainty of the radial and tangential rms velocity components is 4.1% and 9.4% on axis and close to the wall, respectively. The refraction of the beams at the curved optical boundaries was taken into account in the calculations of the measuring volume location, measuring volume orientation and conversion factor, following the equations presented in Durst *et al* [28]. For measurements of the radial component of the velocity, the plane of the laser beams was perpendicular to the pipe axis and the anemometer was traversed sideways, in the normal direction relative to the optical axis.

The velocimeter was mounted on a milling table with movement in the three coordinates and the positional uncertainties are those of table II. The positioning of the control volume was done visually with the help of infrared sensitive screens, video camera and monitor. Any sistematic positional error was corrected by plotting the axial mean velocity profiles, and whenever the assymetry of the flow was greater than half the size of the control volume, that value was added or subtracted to the milling table so that the profile became symmetric. This method was verified by measuring a second time the same velocity profile and seen to produce always a symmetric curve after the correction was applied.

Table I - Laser-Doppler characteristics

Laser wavelength	827 nm
Laser power	100 mW
Measured half angle of beams in air	3.68
Dimensions of measuring volume in water at e^{-2} intensity	
minor axis	37μm
major axis	550μm
Fringe spacing	6.44μm
Frequency shift	2.5 MHz

Table II- Estimates of positional uncertainty

Quantity	Systematic	Random
x,y (horizontal plane) accuracy of milling table	-	± 10 μm
z (vertical) accuracy of milling table	-	±100 μm
x,y (horizontal plane) accuracy of visual positioning	-	±200μm
z (vertical) accuracy of visual positioning	-	± 100 μm

3 - Results and discussion

3 .1- Rheological characterisation

Some polymers of molecular weight below 10,000 kg/kmole were initially selected for preliminary tests on their viscosity, shear-thinning behaviour, suitability for LDA measurements, ease of use and resistance to degradation. 0.5% by weight aqueous solutions of two methil hydroxil celluloses from Hoechst, Tylose MH 10000K and Tylose MHB 3000 P, and one acrylic copolymer from Rohm and Haas, Acrysol TT35, all of them with 0.02% by weight of the biocide Kathon LXE (Rohm and Haas) were prepared with Porto tap water for testing. The Acrysol solution was too opaque to allow the use of Laser Doppler velocimetry, but could be made transparent if buffered with ammonia. As can be seen in figure 1, the viscosity of the Acrysol TT solution was too low and at this concentration didn't have a strong enough shear-thinning behaviour.

The stability of the Tylose solutions was better than that of the Acrysol, as shown by the 3%, 4.6% and 8.5% variations in viscosity with sample ageing of figure 2 with the Tylose MH, Tylose MHB and Acrysol TT solutions, respectively.

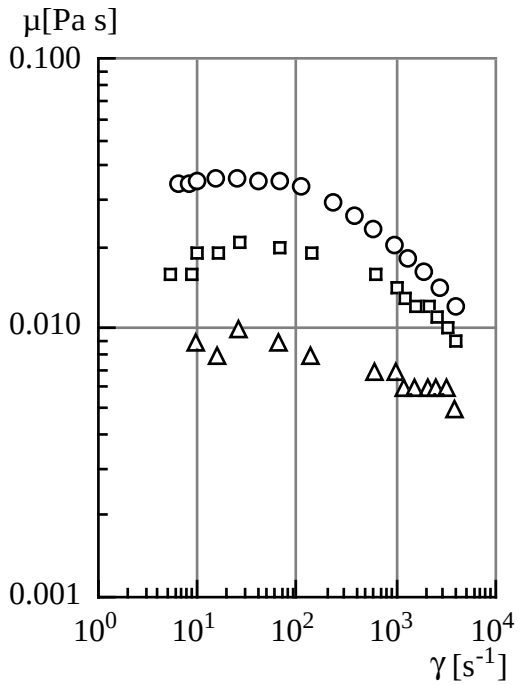

Figure 1 - Viscosity of various fresh samples of 0.5% aqueous polymer solutions at 25˚ C. O Tylose MH; o Tylose MHB; Δ Acrysol TT.

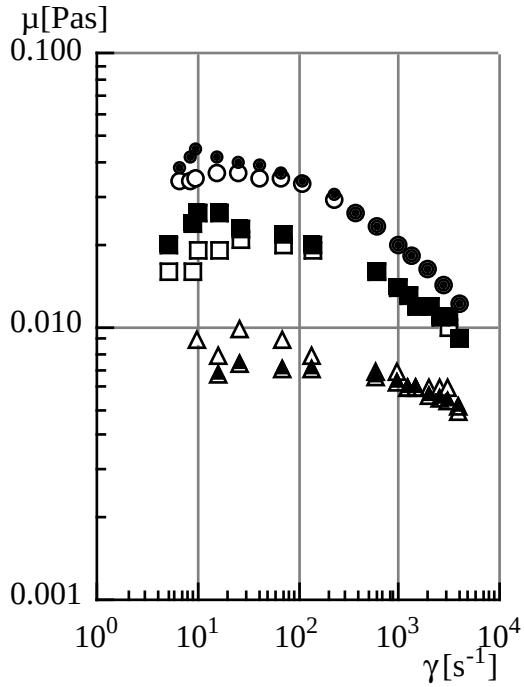

Figure 2- Variation of viscosity of various 0.5% low molecular weight polymer solutions with age. Open symbols- fresh samples. ■ Tylose MH (5 days); ▪ Tylose MHB (11 days); ▲ Acrysol TT (7 days).

The Tylose solutions were sufficiently transparent with the viscosity of the MH 10000K grade better in terms of shear-thinning intensity and still sufficiently low to enable Reynolds number flows in excess of 10000 to occur in the pipe flow rig. Its resistance to degradation, assessed as the time for a 10% decrease in viscometric viscosity, was better than that of Tylose MHB 3000 after 20 hours of flow in the pipe rig at maximum flow rate, as shown in the results of figure 3. From these preliminary experiments the aqueous solutions of Tylose MH 10000K were chosen for having the best set of characteristics. It has a molecular weight of 6,000 and three aqueous solutions of this polymer at concentrations of 0.4%, 0.5% and 0.6% by weight were selected for the hydrodynamic experiments. The viscosity of the three solutions have a clear shear-thinning behaviour with a constant viscosity plateau at low shear rates and a power law variation at high shear rates.

Table III- Parameters of the Carreau model for the viscosity of the Tylose MH 10000K solutions at 25˚ C.

Solução	μ_0 [Pa.s]	λ [s]	n	$\dot{\gamma}$ [s^{-1}]
0.4% Tylose	0.0208	0.0047	0.725	6.1 a 4031
0.5% Tylose	0.0344	0.005	0.660	6.1 a 4031
0.6% Tylose	0.0705	0.0112	0.637	6.1 a 4031

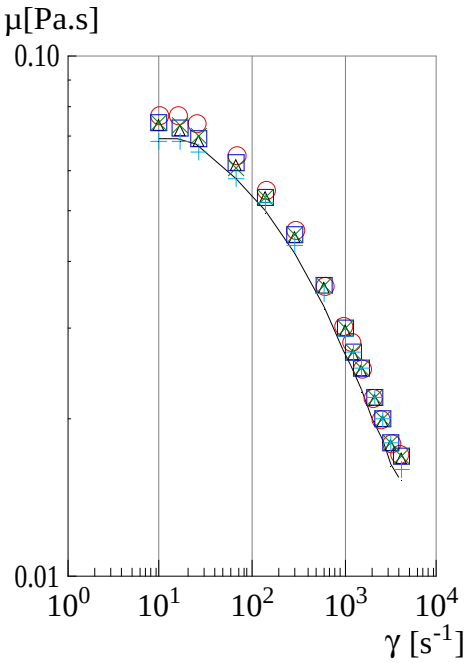

Figure 3- Variation of viscosity of Tylose MH 10000K with shear time in the pipe rig. O 0 hours, Δ 8 hours, ʘ 16 hours, x 20 hours, + 26 hours and — (-10% limit line).

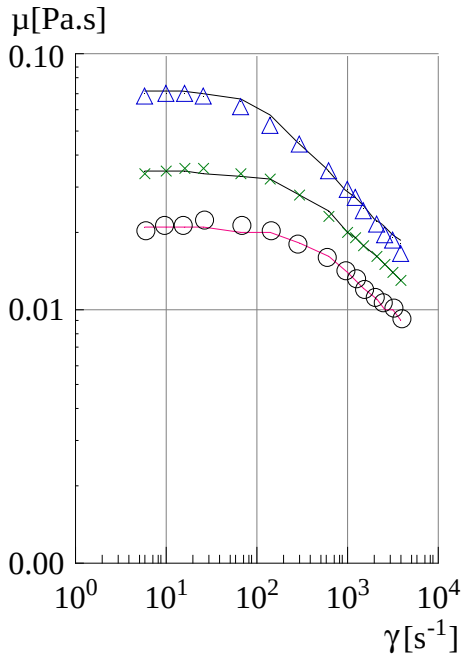

Figure 4- Viscosity and ajusted Carreau model to the 25˚ C Tylose solutions data. O- 0.4%; x-0.5% and Δ- 0.6%.

The Carreau model

$$\mu = \mu_0 \left[1+(\lambda\dot{\gamma})^2\right]^{\frac{n-1}{2}} \quad (1)$$

was fitted with a least-square method to the experimental data at 25˚ C, and its parameters are listed in table III and compared with the data in figure 4.

Measurements of the complex dynamic viscosity in oscillatory shear flow and of the creep factor in creep tests were also carried out in the rheometer for the 0.6% solution, and showed that this solution was almost inelastic. The ratio of the viscous to the elastic component of the complex viscosity was about 10, for frequencies between 1 and 10 Hz, increasing to more than 1,000 above 20 Hz. In the creep tests the transient response to the sudden shearing stress could be barely detected. In conclusion, the aqueous solutions of Tylose can be considered inelastic as measured by the complex viscosity in oscillatory flows and creep tests. These fluids are also prone to mechanical degradation, but under similar conditions have a lifetime 3 times longer than the CMC solutions of molecular weight of 300,000 used by Pinho and Whitelaw [19].

3 .2- Hydrodynamic results

Table IV summarises the main integral quantities of all the runs with water and the Tylose solutions, namely the bulk flow velocity (U_b), normalised center-line velocity (U_0/U_b), the wall viscosity obtained from the measured pressure gradients, the apparent viscosity based on the generalised Reynolds number as defined by Dodge and Metzner [2], the Reynolds number based on wall viscosity and the generalised Reynolds number. The table also includes the drag reduction (DR) relative to the Newtonian friction law at the same wall Reynolds number and the drag reduction intensity relative to the maximum drag reduction predicted by Virk's asymptote. The last column of Table IV is the drag reduction (DR*) relative to the Dodge and Metzner's [2] Darcy friction coefficient law based on the generalised Reynolds number, equation 2:

$$\sqrt{\frac{1}{f}} = \frac{2}{n^{0.75}} \log\left[Re_{gen}\, f^{\frac{2-n}{n}}\right] - \frac{1.204}{n^{0.75}} + 0.602\, n^{0.25} - \frac{0.2}{n^{1.2}} \quad (2)$$

Figures 5 and 6 show the Darcy skin-friction coefficient ($f=2\Delta pD/\rho u_b^2 L$) versus generalised and wall Reynolds numbers respectively, and illustrates the behaviour of the non-Newtonian solutions under laminar, transitional and turbulent flow conditions. The use of the generalised Reynolds number is appropriate in laminar flow and collapses the experimental data on the Newtonian relationship $f=64/Re_{gen}$ within the experimental uncertainty (figure 5), whereas for the turbulent flow data the wall viscosity is preferred

because it is in the wall region that viscous forces are most important. The generalised Reynolds number was calculated with consistency and power indices obtained from the fitting of a power law model to the viscosity data of the solutions, within the shear rate range of each flow condition.

The Newtonian data for the turbulent flow are consistent with previous results and confirm that the flow is close to being fully developed at high Reynolds numbers. Although not conclusive, the drop of the ratio of centreline to bulk velocity (U_o/U_b) with Reynolds number of figure 7 indicates that the flow condition is fully developed, or close to it, for the maximum flow rate with the various polymer solutions.

The two skin friction plots, especially figure 6, clearly emphasize the main conclusion of this work; in spite of the very low molecular weight of Tylose the aqueous solutions of this polymer exhibit drag reduction, and this is consistent with the mean velocity profiles in wall coordinates shown below. The reduction of the friction factor is not a consequence of the shear-thinning characteristic of the polymer solutions as can be seen in figure 5, which compares the measured data with equation 2, the expression derived by Dodge and Metzner [2] for the turbulent flow of shear-thinning inelastic fluids and validated by himself and Hartnett [15], amongst others. For turbulent flow the correct comparison of friction data is on the basis of the wall Reynolds number, but an alternative criteria based on a constant flow rate, again confirms the drag reduction. The flow runs of all the solutions of Table IV at their maximum flow rate, pertain to the same flow condition of fully opened valves. For the water, the maximum bulk velocity was about 4 m/s, whereas for the Tylose solutions it is in excess of 5 m/s, clearly demonstrating a reduction in the friction, in spite of the increased viscosity of the non-newtonian fluids relative to water.

Table IV confirms drag reductions of over 35% and 25% relative to newtonian and pseudoplastic fluids at the same appropriate wall and generalised Reynolds numbers, respectively. These results also show that drag reductions of over 50% of the maximum values predicted by Virk's asymptote are reached by the Tylose solutions, if the comparisons are made on the basis of the wall Reynolds number.

Figure 7 and the data of table IV show that transition from laminar to turbulent flow is somehow delayed by the increased polymer concentration. The 0.4% Tylose flow at a wall Reynolds number of 4,920 seems to be already turbulent, whereas the flows of the 0.5% and 0.6% Tylose at wall Reynolds numbers of 5,220 and 4,860 still have ratios of U_0/U_b higher than 1.3. Although this plot is not conclusive on this issue, which would require a trace of the velocity with time, the flows with higher values of U_0/U_b also have turbulence intensities which are higher than those at higher Reynolds numbers, and that

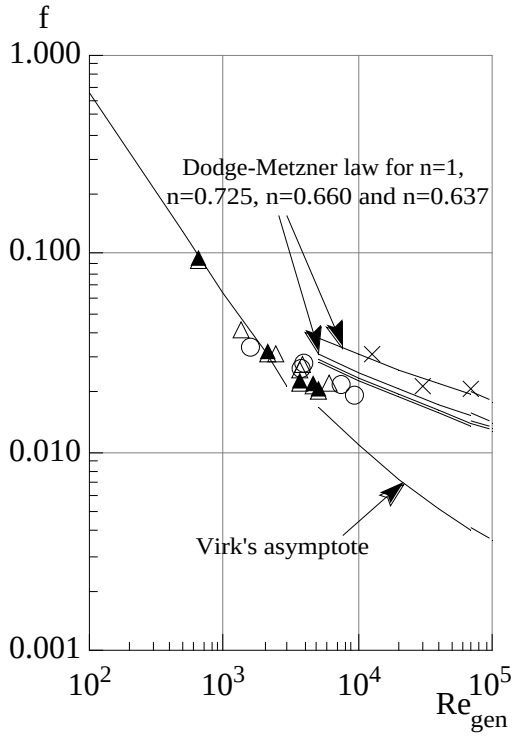

Figure 5- Darcy friction factor versus generalised Reynolds number. X Water, O Tylose 0.4%, Δ Tylose 0.5% and ѕ Tylose 0.6%.

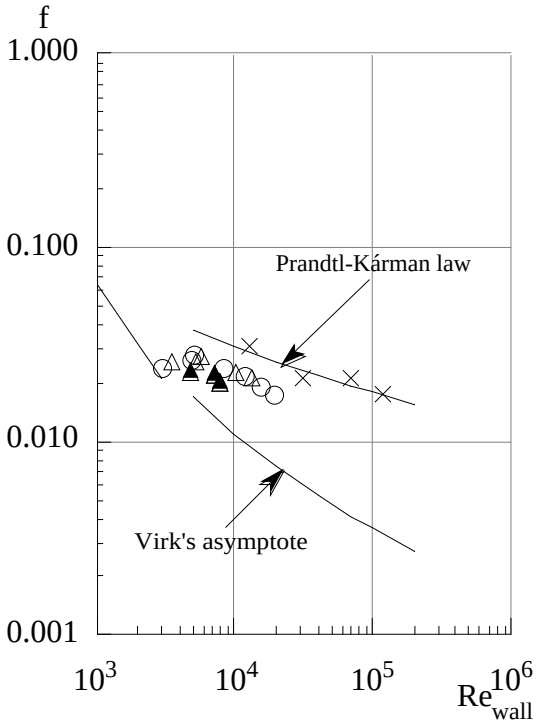

Figure 6- Darcy friction factor versus wall Reynolds number. X Water, O Tylose 0.4%, Δ Tylose 0.5% and ѕ Tylose 0.6%.

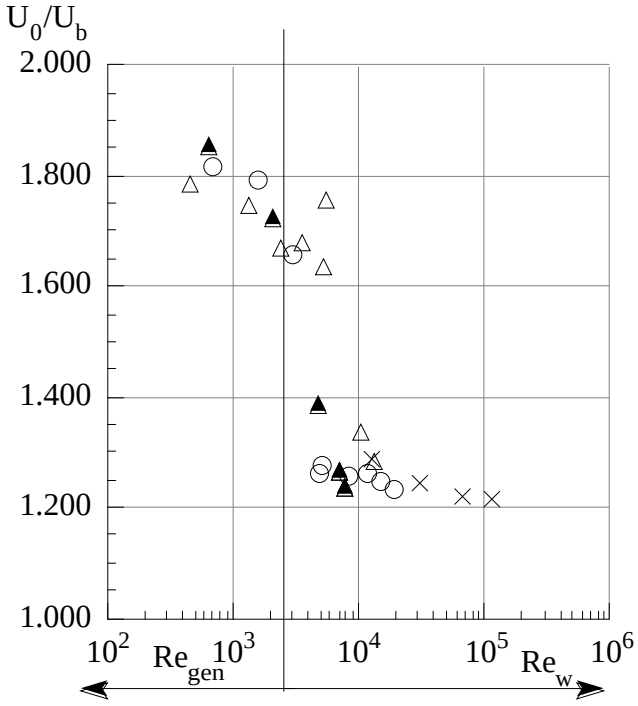

Figure 7- Ratio of centreline to bulk velocity versus generalized and wall Reynolds number for X Water, O Tylose 0.4%, Δ Tylose 0.5% and ѕ Tylose 0.6%.

can be due to flow intermittency. It is not surprising to observe a non-Newtonian effect on transition which has been beautifully reported in the past by Wójs [29], amongst others.

Table IV- Main integral flow characteristics (Water and Tylose solutions)

Fluid	U_b[m/s]	U_0/U_b	μ_w [Pa.s]	μ_{ap} [Pa.s]	Re_w	Re_{gen}	DR [%]	DR/DR_{max}	DR* [%]
Water	4.04	1.21	0.000894	0.000894	117,400	117,400	-	-	-
Water	2.36	1.22	0.000894	0.000894	68700	68,700	-	-	-
Water	1.07	1.24	0.000894	0.000894	31,100	31,100	-	-	-
Water	0.45	1.29	0.000894	0.000894	13,100	13,100	-	-	-
0.4%	5.59	1.23	0.00742	0.0125	19,570	11,660	34.1	47.7	28.5
0.4%	4.76	1.25	0.00804	0.0130	15,400	9,500	30.7	44.2	24.7
0.4%	4.01	1.26	0.00873	0.0136	11,930	7,640	26.4	39.5	19.9
0.4%	3.21	1.26	0.00993	0.0144	8,400	5,790	25.7	40.9	18.4
0.4%	2.32	1.26	0.0123	0.0157	4,920	3,860	30.6	56.4	22.1
0.4%	1.79	1.66	0.0153	0.0165	3,030	2,820	-	-	-
0.4%	1.13	1.79	0.0178	0.0184	1,660	1,600	-	-	-
0.4%	0.54	1.82	0.0201	0.0198	700	707	-	-	-
0.5%	5.16	1.29	0.0101	0.0182	13,260	7,360	22.7	33.4	14.0
0.5%	4.51	1.34	0.0113	0.0191	10,360	6,160	23.9	36.6	14.6
0.5%	3.11	1.64	0.0155	0.0216	5,220	3,730	27.6	49.8	16.4
0.5%	2.57	1.68	0.0188	0.0230	3,560	2,900	-	-	-
0.5%	2.23	1.67	0.0196	0.0241	2,950	2,410	-	-	-
0.5%	1.41	1.75	0.0260	0.0272	1,410	1,350	-	-	-
0.5%	0.56	1.79	0.0314	0.0316	467	464	-	-	-
0.6%	5.31	1.24	0.0174	0.0267	7,950	5,180	36.6	59.0	26.0
0.6%	4.95	1.27	0.0181	0.0274	7,100	4,700	34.3	56.8	23.3
0.6%	4.10	1.39	0.0219	0.0293	4,860	3,640	38.6	54.1	26.7
0.6%	2.80	1.73	0.0279	0.0337	2,600	2,160	-	-	-
0.6%	1.14	1.86	0.0418	0.0461	710	644	-	-	-

Local measurements of the mean velocity and of the root-mean-square of the velocity fluctuations of the 0.4, 0.5% and 0.6% by weight Tylose MH 10000K solutions are shown in figures 8 to 10 which sometimes include non-Newtonian data taken from Pinho and Whitelaw [19] concerning aqueous solutions of CMC (sodium carboxymethil cellulose) grade 7H4C from Hercules with a molecular weight of around $3x10^5$, i.e., about 50 times heavier than the Tylose solutions used in this work. Table V summarises for these flows the same type of information presented in Table IV.

The axial mean velocity profile of the 0.4% Tylose at a Reynolds number of 3,030 in figure 8 a) is clearly not turbulent. The flow at the Reynolds number of 4,920, in spite of a low value of the ratio U_0/U_b in figure 7 which could indicate turbulent flow, does not seem to be under such flow condition as the exceedingly high velocity fluctuations of figures 8c) to e) suggest. For this flow condition the turbulence is much higher than that for higher Reynolds number, and this can be associated with flow intermittency. Normal Reynolds stresses increase gradually with the decrease in Reynolds number, Wei and Willmarth [31], but for this low Reynolds number range the variations should not be so intense as observed here unless the flow is within a transitional condition with intermittency contributing decisively to turbulence broadening.

Table V - Main integral flow characteristics of CMC solutions (from Pinho and Whitelaw [19])

Fluid	U_b[m/s]	U_0/U_b	μ_w [Pa.s]	μ_{ap} [Pa.s]	Re_w	Re_{gen}	DR [%]	DR/DR_{max}
0.1%	5.12	1.19	0.00306	0.00380	43,000	34,200	59.8	77.8
0.1%	3.28	1.23	0.00331	0.00395	25,200	21,100	53.0	71.6
0.1%	2.28	1.24	0.00345	0.00412	16,800	14,060	46.8	67.6
0.1%	1.30	1.25	0.00375	0.00438	8750	7530	20.5	32
0.2%	5.10	1.25	0.00520	0.00700	30,000	18,500	65.6	87.1
0.2%	3.99	1.35	0.00555	0.00750	18,260	13510	65.0	90.6
0.2%	3.11	1.39	0.00670	0.00800	11,770	9860	64.0	94.4

The axial mean velocity profiles in wall coordinates of the 0.4% Tylose solutions in figure 8 b) are consistent with the drag reduction because they are shifted upwards from the newtonian log law proportionally to the drag reduction intensity. This is better understood from the comparison with the 0.1% and 0.2% CMC data of Pinho and Whitelaw [19] which were reported to have drag reductions of 47% and 64%, respectively. The more intense drag reductions of these heavy polymers imply a larger shift from the newtonian log law than that of the light Tylose solutions. Figure 8 b) also shows that the slope of the velocity profiles become steeper with drag reduction, especially at higher values of drag reduction, close to Virk's asymptote.

The normal Reynolds stresses of the Tylose solutions have a behaviour intermediate to the newtonian and the high molecular weight and intense drag reducer CMC solutions. The axial component of the Reynolds stress of the 0.4% Tylose solutions is not so high close to the wall as with the 0.2% CMC solutions, the one that is closer to the 0.4% Tylose in terms of viscous characteristics, and at the centre of the pipe the turbulence is not so damped, as shown in figure 8 c). Drag reduction is known to intensify axial turbulence near the wall (Allan *et al* [10]) and is associated with a decrease of transverse turbulent transport. With drag reductions which are intermediate

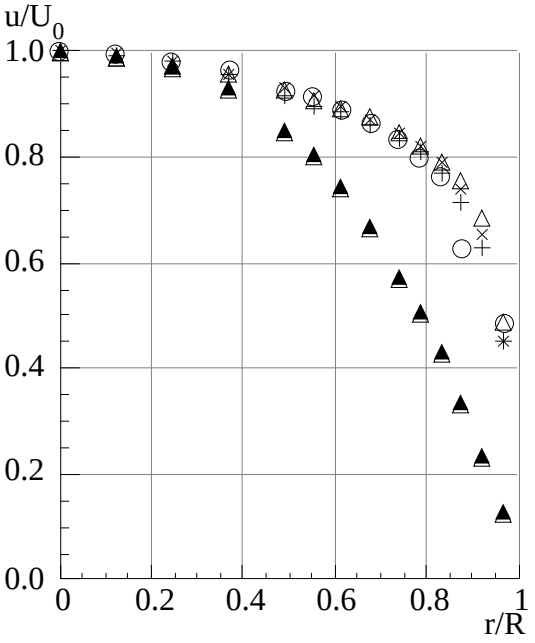

Figure 8a) Axial mean velocity profile in physical coordinates for the 0.4% Tylose solutions. s Re_w= 3030, O Re_w= 4920, + Re_w= 11930, X Re_w= 15400 and Δ Re_w= 19570.

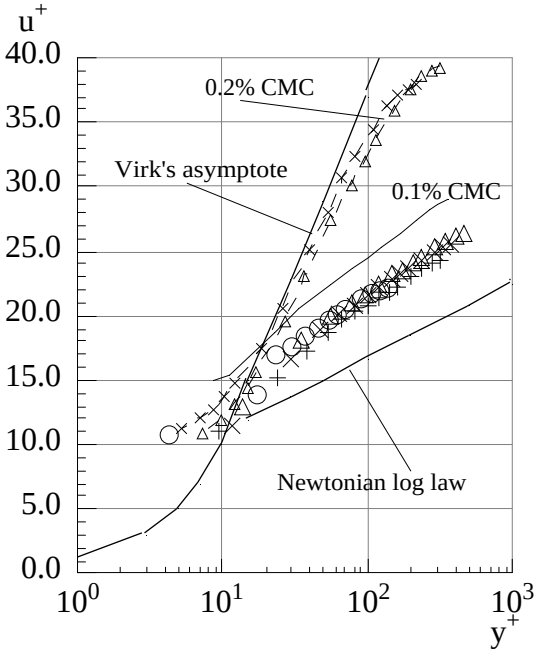

Figure 8b) Axial mean velocity profile in wall coordinates for the 0.4% Tylose solutions. O Re_w= 4920, + Re_w= 11930, X Re_w= 15400 and Δ Re_w= 19570. From Pinho and Whitelaw [19] -Δ-Δ- 0.2% CMC at Re_w= 18260,-x-x- 0.2% CMC at Re_w= 11770,—— 0.1% CMC at Re_w= 16800.

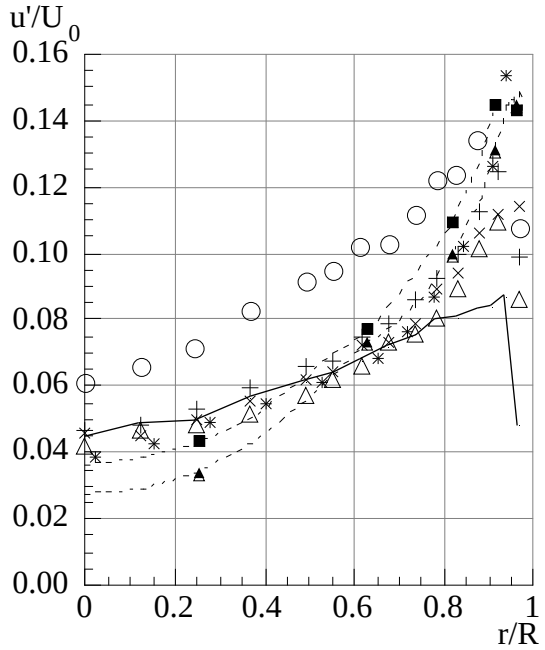

Figure 8c) Axial rms velocity profile in physical coordinates for the 0.4% Tylose solutions. O Re_w= 4920, + Re_w= 11930, X Re_w= 15400 and Δ Re_w= 19570. —— Water Re= 117500. From Pinho and Whitelaw [19] -s- 0.2% CMC at Re_w= 18260,- n - 0.2% CMC at Re_w= 11770, * 0.1% CMC at Re_w= 16800.

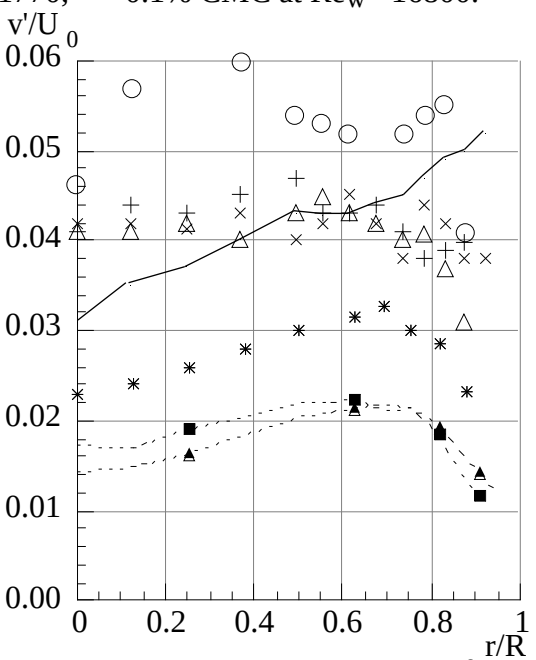

Figure 8d) Radial rms velocity profile in physical coordinates for the 0.4% Tylose solutions. O Re_w= 4920, + Re_w= 11930, X Re_w= 15400 and Δ Re_w= 19570. —— Water Re= 117500. From Pinho and Whitelaw [19] -s- 0.2% CMC at Re_w= 18260,- n - 0.2% CMC at Re_w= 11770, * 0.1% CMC at Re_w= 16800.

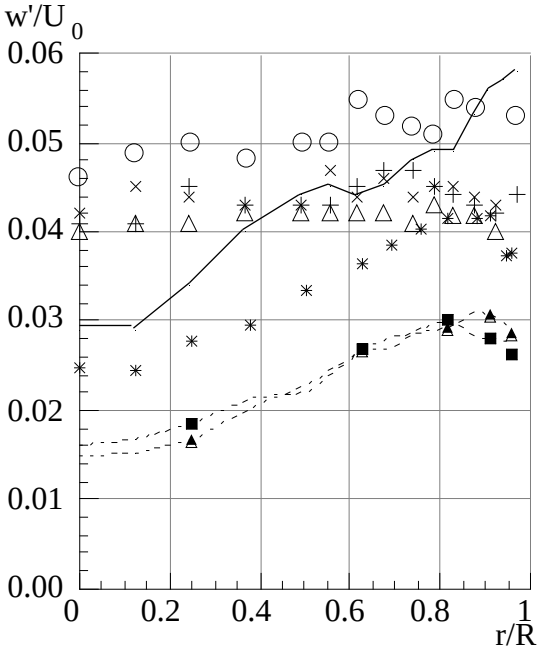

Figure 8e) Azimuthal rms velocity profile in physical coordinates for the 0.4% Tylose solutions. O Re_w= 4920, + Re_w= 11930, X Re_w= 15400 and Δ Re_w= 19570. —— Water Re= 117500. From Pinho and Whitelaw [19] -s- 0.2% CMC at Re_w= 18260,- n - 0.2% CMC at Re_w= 11770, * 0.1% CMC at Re_w= 16800.

between those of the CMC solutions and the newtonian fluid, it is expected that the profiles of the rms velocities reflect this behaviour, as happens here. The axial turbulence profiles show a small Reynolds number effect with the flow at a Reynolds number of 11,930 having marginally higher values than the flow at a higher Reynolds number.

The radial and azimuthal components of the rms of the fluctuating velocity of the 0.4% Tylose fluids in figures 8 d) and e) agree with the previous observations, showing less dampening than those of the CMC solutions. However there is a major difference between the Tylose and the CMC curves: although intense dampening of the transverse turbulence is observed with the Tylose and CMC solutions in the near-wall region in relation to the water flows, in the centre of the pipe there is no reduction of turbulence with the Tylose, and in fact the opposite occurs. Radial and tangential rms velocities hardly increase from the centre of the pipe to the wall, remaining almost constant within 80% of the radius, and decreasing only on the final 20% near the wall. The high radial and tangential turbulence in the center of the pipe could be due to the reported delay in transition together with a Reynolds number effect. This means that Reynolds number and transitional effects with the Tylose solutions occur over a wider range of Reynolds numbers than with the water flows. For the water flows at Reynolds numbers between

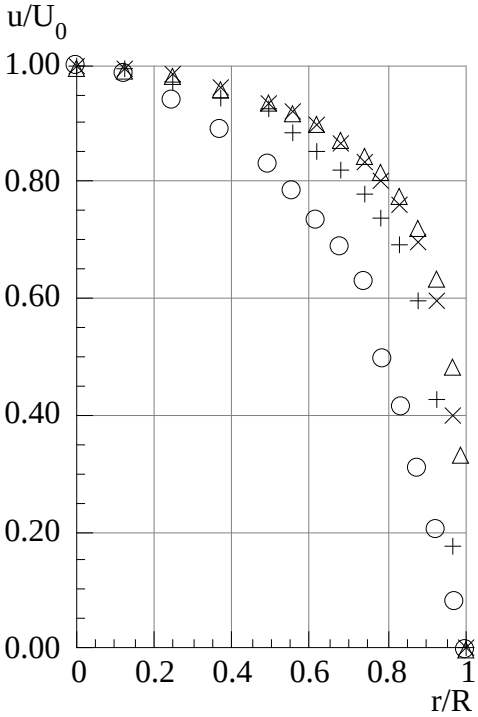

Figure 9a) Axial mean velocity profile in physical coordinates for the 0.6% Tylose solutions. O Re_w= 2160, + Re_w= 4860, X Re_w= 7100 and Δ Re_w= 7950.

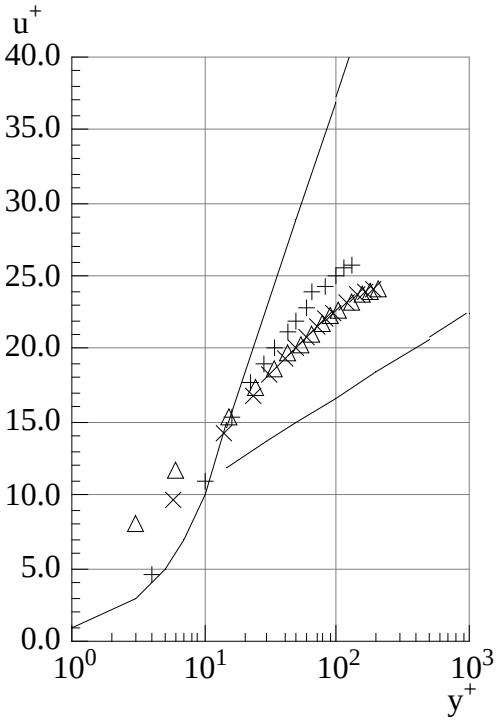

Figure 9b) Axial mean velocity profile in wall coordinates for the 0.6% Tylose solutions. O Re_w= 2160, + Re_w= 4860, X Re_w= 7100 and Δ Re_w= 7950.

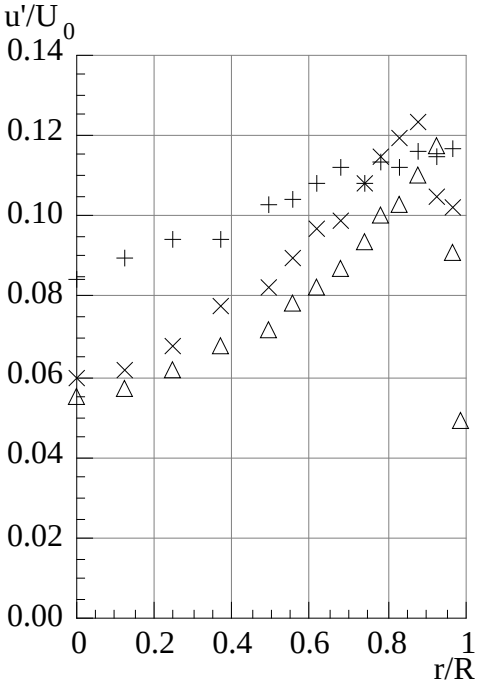

Figure 9c) Axial rms velocity profile in wall coordinates for the 0.6% Tylose solutions. + Re_w= 4860, X Re_w= 7100 and Δ Re_w= 7950.

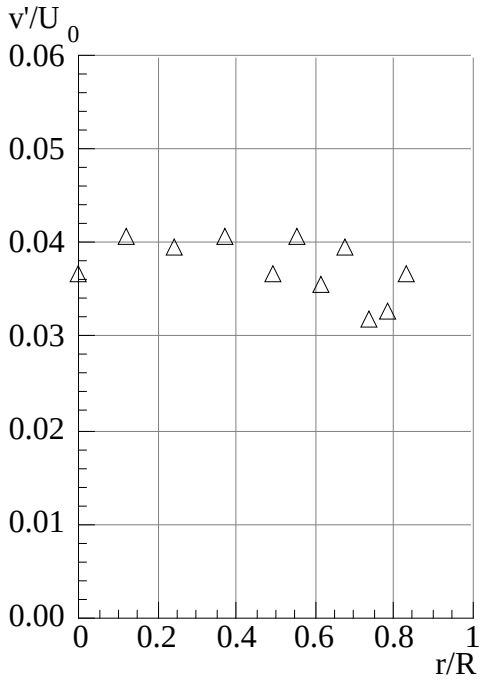

Figure 9d) Radial rms velocity profile in wall coordinates for the 0.6% Tylose solutions. Δ Re_w= 7950.

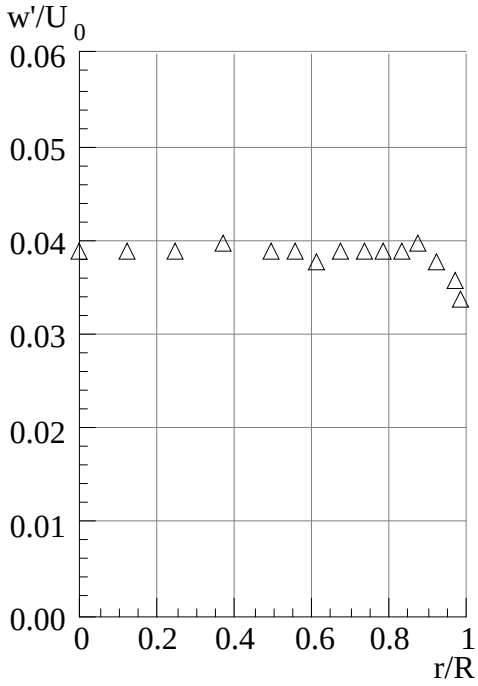

Figure 9e) Azimuthal rms velocity profile in wall coordinates for the 0.6% Tylose solutions. Δ Re_w= 7950.

30,000 and 117,500 the turbulence profiles hardly change, and agree well with data from Lawn [30] indicating fully developed turbulent flow in all conditions. Besides, as already mentioned, Reynolds number effects with newtonian fluids are not so intense as observed here with the non-newtonian fluids.

It is clear that the effects of drag reduction on the turbulence characteristics of the low molecular weight polymers are localised in the wall region, whereas for the high molecular weight solutions they span over the whole pipe, and this effect is not restricted to the transverse components of turbulence. In the centre of the pipe the axial component of turbulence of the Tylose solutions is similar to the newtonian values whereas the CMC axial turbulence intensity is attenuated.

Of the various theories that were developed to explain drag reduction, Kostic [32], the most convincing attributes this phenomena to the rise of the extensional viscosity asociated with the elongational molecular deformation, also called molecular stretching, by the turbulent flow field, and its effect upon the dissipative eddies and turbulence, Lumley [33] and Tabor *et al* [23]. It is this effect that is referred throughout this paper by the authors, as the elasticity responsible for drag reduction.

One can only speculate, but the opposite observations of the behaviour of Tylose and CMC could be the result of two different elastic effects: elongational elasticity, due to increased resistance of molecules to molecular stretching, dampens turbulence, reduces

transverse momentum transfer and therefore contributes to drag reduction, but simultaneously it delays transition thus raising turbulence. The intensity of the drag reduction effect tends to be dominant with solutions of large, heavy molecules, regardless of the polymer concentration, whereas the latter occurs with more concentrated solutions, i.e., it depends more on polymer concentration. In fact, very dilute solutions of heavy molecules are known to reach Virk's maximum drag reduction asymptote, only after a normal transition from laminar to turbulent flow and an onset of drag reduction well over the Colebrooke- White friction factor law. With more concentrated solutions, this onset takes place earlier, before transition, under laminar flow conditions and the sudden increase of friction factor typical of transitional behaviour is not observed. This was concluded by Virk *et al* [6], who showed that each polymer had a single value of a critical wall shear stress at which the onset of drag reduction took place. An early onset of drag reduction is responsible for the delayed transition and this dual behaviour was also observed by Pinho and Whitelaw (1990) with their CMC experiments: the onset of drag reduction for the 0.1% CMC took place after transition, but for the higher CMC concentrations the onset occurred over the laminar law.

In this work a small molecule was investigated, but at higher concentrations than the CMC solutions of Pinho and Whitelaw [19], so that both solutions have comparable viscosity behaviour. The Tylose solutions exhibit drag reduction together with delayed transition, i.e., the onset of drag reduction is over the 64/Re friction factor equation. This behaviour is opposed to the typical turbulent flow drag reduction of very dilute aqueous solutions of long molecules, such as polyacrilamide or polyethylene oxide solutions. The turbulent flow of these long molecules show low normal Reynolds stresses coupled with an onset of drag reduction on the Colebrooke- White equation for friction factor, after a proper transition to turbulent flow has taken place. The Tylose solutions exhibits the mixed behaviour of a delayed transition and drag reduction, but it is not possible to quantify separately each of these contributions.

The measurements with the 0.6% Tylose in figure 9 also show the delay in transition. The flow at a Reynolds number of 4,860 is not turbulent and the flow at a Reynolds number of 7,100 has features of normal Reynolds stress similar to the 4,920 Reynolds number flow of the 0.4% Tylose, i.e., higher turbulence than the flow at a Reynolds number of 8,000.

Finally, figure 10 compares mean and rms velocity data between the Tylose solutions, the 0.2% CMC and the water flows at a Reynolds number of about 12,000, with two exceptions: the water flow condition is at a Reynolds number of 31,000 and the Reynolds number for the 0.6% Tylose flow is 7,950 corresponding to the maximum a-

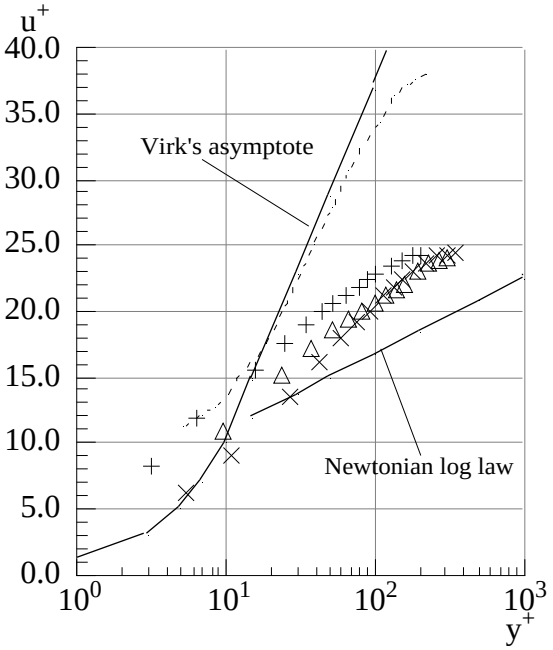

Figure 10 a) Law of the wall for the Tylose and 0.2% CMC solution of Pinho and Whitelaw [19] at $Re_w \approx$ 12,000. Δ 0.4% Tyl. Re= 11930; X 0.5% Tyl. Re= 13260, + 0.6% Tyl. Re= 7950. - - - 0.2%CMC Re= 11770.

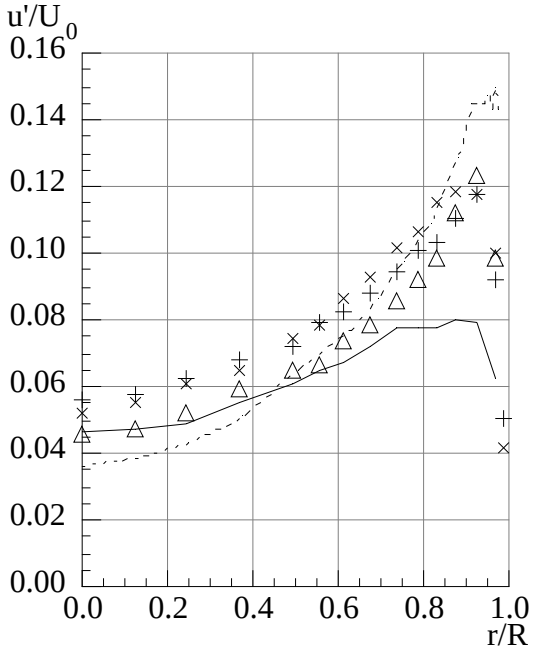

Figure 10 b) Rms of the axial velocity component for the Tylose and 0.2% CMC solution of Pinho and Whitelaw [19] at $Re_w \approx$ 12,000. Δ 0.4% Tyl. Re= 11930; X 0.5% Tyl. Re= 13260, + 0.6% Tyl. Re= 7950. - - - 0.2%CMC Re= 11770,—— water Re= 31000.

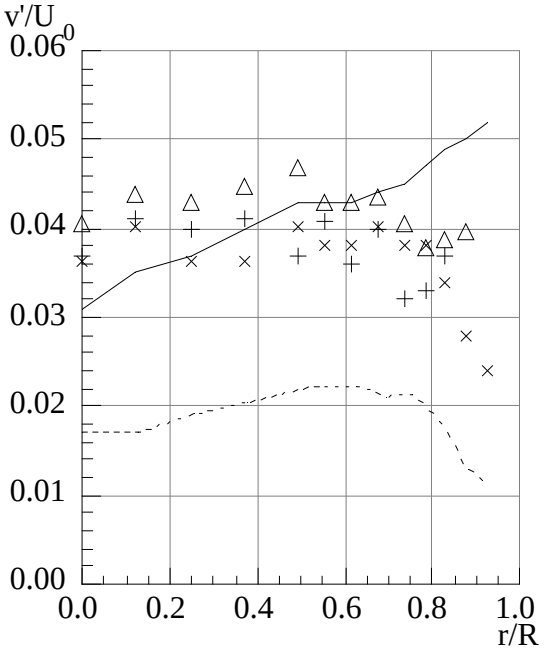

Figure 10 c) Rms of the radial velocity component for the Tylose and 0.2% CMC solution of Pinho and Whitelaw [19] at $Re_w \approx$ 12,000. Δ 0.4% Tyl. Re= 11930; X 0.5% Tyl. Re= 13260, + 0.6% Tyl. Re= 7950. - - - 0.2%CMC Re= 11770,—— water Re= 31000.

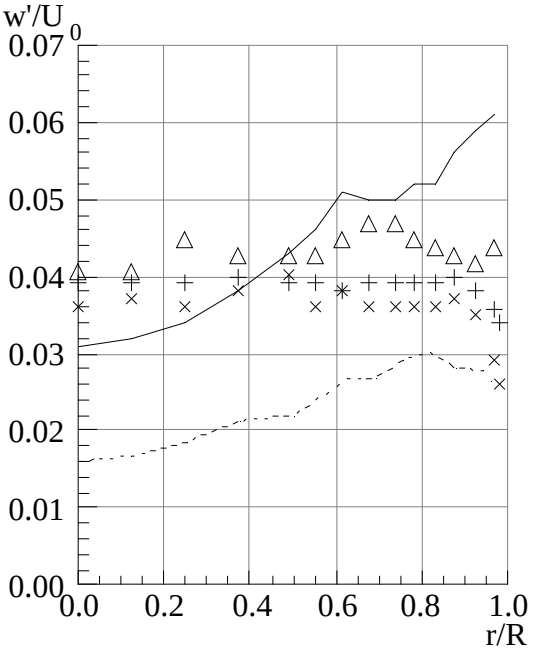

Figure 10 d) Rms of the azimuthal velocity component for the Tylose and 0.2% CMC solution of Pinho and Whitelaw [19] at $Re_w \approx$ 12,000. Δ 0.4% Tyl. Re= 11930; X 0.5% Tyl. Re= 13260, + 0.6% Tyl. Re= 7950. - - - 0.2%CMC Re= 11770,—— water Re= 31000.

chievable flow rate with this fluid. The variation of the turbulence characteristics of newtonian fluids with Reynolds numbers between 31,000 and 12,000 is small according to Wei and Willmarth [31], so that this data can be considered accurate enough for this comparison. The profiles of figure 10 and their variations are consistent with the arguments put forward before; axial mean velocity profiles in wall coordinates are shifted upward from the newtonian log law proportionally to the drag reduction intensity, the axial turbulence intensity is higher than the water values close to the wall for the more intense drag reducers, and the dampening of the transverse components of turbulence is also proportional to the reduction of the friction coefficient. The transverse components of turbulence with the Tylose solutions are again dampened only in the wall region whereas for the CMC solution it occurs everywhere.

Berman [20] showed that in polydisperse polymer solutions the main contribution to drag reduction comes from the higher molecular weight molecules. Hoechst, the manufacturer of Tylose, could not report on its molecular weight distribution, and one may be lead to conclude that the observed drag reduction results from the high molecular weight molecules that are certainly present in these samples. However, if the size distribution of Tylose is as wider as in heavier polymer samples reported in the literature, the larger molecules of Tylose are smaller than the smaller molecules of high molecular weight fluids investigated in the past, and the observed drag reduction can be truly attributed to these light molecules. This is also confirmed by the lower maximum DR that was achieved with Tylose, in spite of the high polymer concentrations, when compared with drag reductions involving CMC and other high molecular weight solutions [6-11].

The dependence of drag reduction on pipe diameter has made it hard to formulate appropriate procedures to scale up and down this effect in the past, Hoyt [34], but recently Hoyt and Sellin [35] proposed and demonstrated an accurate method where the reduced friction is made equivalent to a negative roughness on the White-Colebrook friction law. It is important to have relations for the scaling of any drag reducing fluid that can be used industrially, and the good resistance to degradation of the solutions of Tylose grade MH 10000K from Hoechst coupled with their drag reducing capabilities make them good candidates. The following equations can be used to predict the friction factor (f_2) as a function of the Reynolds number (Re_2) in pipes of diameter (D_2) with the 0.4 and 0.6% by weight aqueous Tylose solutions from the data measured in this work (f_1, Re_1 and D_1 = 26 mm). The friction factor f_2 is given by equation 3

$$\frac{1}{\sqrt{f_2}} = -2.0 \log\left[\frac{D_2}{D_1}\mathbf{A}\right] \qquad (3)$$

with the corresponding Reynolds number (Re_2) calculated from the following relationship.

$$Re_2 = Re_1 \frac{D_2}{D_1} \frac{\log\left[\frac{D_2}{D_1}\mathbf{A}\right]}{\log[\mathbf{A}]} \quad (4)$$

Table VI - White-Colebrook kernel **A** for the 0.4 and 0.6% Tylose solutions in water.

Fluid	**A**	Reynolds number (Re_1) range
0.4% Tylose	$0.00193 \quad e^{-0.000132Re_1}$	5,200 to 19,600
0.6% Tylose	$0.000997\ e^{-0.000126Re_1}$	4,800 to 8,000

A is a function of the solution, drag reduction and Reynolds number, and the equations in Table VI were obtained by fitting experimental data with a the least-square fitting method.

4- Conclusions

Aqueous solutions of low molecular weight Tylose (6,000 kg/kmole) are sufficiently transparent to allow measurements with laser velocimetry in depths of field of up to 26 mm, but were found to be less transparent than the 300,000 kg/kmole CMC solutions of Pinho and Whitelaw [19]. In order to have a clear shear-thinning behaviour the concentration of the polymer had to be of 0.4% by weight at least, and the viscosity was constant within 10%, when the fluid was circulated in a closed loop with a centrifugal pump for a periods of over 20 hours, meaning a three fold increase in the resistance to degradation compared with the equivalent viscous heavy CMC solutions. The rheological measurements could not detect any elasticity but the hydrodynamic tests showed elastic effects through drag reductions of 29% to 35% for the 0.4% and 0.6% solutions, respectively.

The turbulence of the Tylose solutions was intensified in the axial direction and reduced in both transverse components relative to turbulent newtonian flows, but these effects only occurred close to the wall, and were not so intense as previously reported with solutions of high molecular weight polymers. In the central region of the pipe turbulence was higher than with water flows, especially in the radial and tangential directions, because of delayed transition due to shear-thinning and molecular stretching effects.

As a drag reducer additive Tylose is less efficient than high molecular weight polymers, but whenever long time exposure to strain is required this polymer should be considered, because of its high resistance to mechanical degradation. Equations for predicting the pressure loss of the Tylose solutions in pipes of different diameter, in the turbulent regime, were derived,following the procedure of Hoyt and Sellin [35].

From this work, the authors are convinced that the prospects of finding inelastic drag reducing shear-thinning fluids based on linear and low crosslinked polymer molecules are scarce. We also conclude, that in the absence of elongational viscosity measurements, it is necessary to complement the traditional rheological characterisation of non-newtonian fluids, with preliminary turbulent pipe flow measurements, whenever a research on any turbulent non-newtonian flow is undertaken.

Acknowledgements

The authors are glad to acknowledge the support of Instituto Nacional de Investigação Científica- INIC, Instituto de Engenharia Mecânica e Gestão Industrial- INEGI and Laboratorio de Hidráulica da Faculdade de Engenharia in financing the rig, lending some equipment and for providing building space for the rig, respectively. We also would like to thank Hoechst, Portugal and Horquim, Portugal for offering us the polymers and additives.

References

1. Metzner, A. B. and Reed, J. C.. Flow of Non-Newtonian Fluids - Correlation of Laminar, Transition and Turbulent Flow Regimes. AIChEJ 1 (1955) 434
2. Dodge, D. W. and Metzner, A. B.. Turbulent Flow of Non-Newtonian Systems. AIChEJ 5 (1959) 189
3. Toms, B. A.. Some Observations on The Flow of Linear Polymer Solutions Through Straight Tubes at Large Reynolds Numbers. Proc. 1st Conf. on Rheol, North Holland Publ. Co., II (1948) 135
4. Logan, S. E.. Laser Velocimeter Measurements of Reynolds Stress and Turbulence in Dilute Polymer Solutions. AIAA J. 10 (1972) 962
5. Donohue, G. L., Tiederman, W. G. and Reischman, M. M.. Flow Visualisation of the Near-Wall Region in Drag Reducing Channel Flows. J. Fluid Mech. 56 (1972) 559
6. Virk, P. S., Merril, E. W., Mickley, H. S., Smith, K. A. and Mollo-Christensen, E. L.. The Tom's Phenomena in Turbulent Pipe Flow of Dilute Polymer Solutions. J. Fluid Mech. 30 (1967) 305
7. Virk, P. S., Mickley, H. S. and Smith, K. A.. The Ultimate Asymptote and Mean Flow Structure in Tom's Phenomena. J. Appl. Mech. 37 (1970) 488
8. Reischman, M. M. and Tiederman, W. G.. Laser-Doppler Anemometer Measurements in Drag-Reducing Channel Flows. J. Fluid Mech. 70 (1975) 369
9. Achia, B. V. and Thompson, D. W.. Structure of the Turbulent Boundary in Drag-Reducing Pipe Flow. J. Fluid Mech. 81 (1977) 439

10. Allan, J. J., Greated, C. A. and McComb, W. D.. Laser-Doppler Anemometer Measurements of Turbulent Structure in Non-Newtonian Fluids. J. Phys. (D): Apply. Phys. 17 (1984) 533
11. Tiederman, W. G., Luchik, T. S. and Bogard, D. G.. Wall-Layer Structure and Drag Reduction. J. Fluid Mech. 156 (1985) 419
12. Luchik, T. S. and Tiederman, W. G.. Turbulent Structure in Low Concentration Drag-Reducing Channel Flows. J. Fluid Mech. 190 (1988) 241
13. Shaver, R. G. and Merril, E. W.. Turbulent Flow of Pseudoplastic Polymer Solutions in Straight Cylindrical Tubes. AIChEJ. 5 (1959) 181
14. Metzner, A. B. and Park, M. G.. Turbulent Flow Characteristics of Viscoelastic Fluids. J. Fluid Mech. 20 (1964) 291
15. Hartnett, J. P.. Viscoelastic Fluids: A New Challenge in Heat Transfer. Trans. ASME: J. Heat Transfer 114 (1992) 296
16. Edwards, M. F. and Smith, R.. The Turbulent Flow of Non-Newtonian Fluids in The Absence of Anomalous Wall Effects. J. N-Newt. Fluid Mech. 7 (1980) 77
17. Park, J. T., Grimley, T. A. and Mannheimer, R. J.. Turbulent Velocity Profile LDA Measurements in Pipe Flow of a Non-Newtonian Slurry with a Yield Stress. Proc. 6th Int. Symp. on Appl. Laser Techniques to Fluid Mech., Lisbon (1992) 33.2
18. Escudier, M. P., Jones, D. M. and Gouldson, I.. Fully Developed Pipe Flow of Shear-Thinning Liquids. Proc. 6th Int. Symp. on Appl. Laser Techniques to Fluid Mech., Lisbon (1992) 1.3
19. Pinho, F. T. and Whitelaw, J. H.. Flow of Non-Newtonian Fluids in a Pipe. J. N-Newt. Fluid Mech. 34, (1990) 129
20. Berman, N. S.. Drag Reductions of the Highest Molecular Weight Fractions of Polyethylene Oxide. Phys. Fluids 20 (1977) 715
21. Burger, E., Munk, W. and Wahl, H.. Flow Increase in The Trans-Alaska Pipeline Using a Polymeric Drag Reducing Additive. Society of Petroleum Engineers, SPE 9419 (1981)
22. Hinch, E. J.. Mechanical Models of Dilute Polymer Solutions in Strong Flows. Phys. Fluids 20 (1977) S22
23. Tabor, M., Durning, C. J. and O'Shaughnessy, B.. The Microscopic Origins of Drag Reduction. Internal Report of University of Columbia, Depts. of Applied Physics, Applied Chemistry and Chem. Eng., NY 10027 (1989)
24. Lodes, A. and Macho, V.. The Influence of PVAC Additive in Water on Turbulent Velocity Field and Drag Reduction. Exp. in Fluids 7 (1989)
25. Pereira, A. S.. Rheologic and Hydrodynamic Characteristics of Low Molecular Weight Non-Newtonian Fluids in Pipe Flows. MSc. Thesis (in Portuguese), Univ. Porto (1993)
26. White, F. M.. Viscous Fluid Flow. 2nd edition, Mc Graw-Hill, New York (1991)

27. Stieglmeier, M. and Tropea, C.. A Miniaturized, Mobile Laser- Doppler Anemometer, Applied Optics 31 (1992) 4096
28. Durst, F., Melling, A. and Whitelaw, J. H.. Principles and Practice of Laser-Doppler Anemometry. 2nd edition, Academic Press (1981)
29. Wójs, K.. Laminar and Turbulent Flow of Dilute Polymer Solutions in Smooth and Rough Pipes. J. N-Newt. Fluid Mech.48 (1993) 337
30. Lawn, C. J. The Determination of the Rate of Dissipation in Turbulent Pipe Flow. J. Fluid Mech. 48 (1971) 477
31. Wei, T. and Willmarth, W. W.. Reynolds Number Effects on The Structure of a Turbulent Channel Flow. J. Fluid Mech. 204 (1989) 57
32. Kostic, M.. On Turbulent Drag and Heat Transfer Reduction Phenomena and Laminar Heat Transfer Enhancement in Non-Circular Duct Flow of Certain Non-Newtonian Fluids. Int. J. Heat Mass Tranfer. 37 (1994) 133
33. Lumley, J. L.. Drag Reduction in Two-Phase and Polymer Flows. Phys. of Fluids 20 (1977) S64
34. Hoyt, J. W.. The Effect of Additives on Fluid Friction. Trans. ASME: J. Basic Eng.94 (1972) 258
35. Hoyt, J. W. and Sellin, R. H. J.. Scale Effects in Polymer Solution Pipe Flow. Exp. in Fluids 15 (1993) 70-74

Legends of figures

Figure 1 - Viscosity of various fresh samples of 0.5% aqueous polymer solutions at 25˚C. O Tylose MH; o Tylose MHB; Δ Acrysol TT.

Figure 2- Variation of viscosity of various 0.5% low molecular weight polymer solutions with age. Open symbols- fresh samples. l Tylose MH (5 days); n Tylose MHB (11 days); s Acrysol TT (7 days).

Figure 3- Variation of viscosity of Tylose MH 10000K with shear time in the pipe rig. O 0 horas, Δ 8 horas, o 16 horas, x 20 horas, + 26 horas and — (-10% limit line).

Figure 4- Viscosity and ajusted Carreau model to the 25˚ C Tylose solutions data. O- 0.4%; x-0.5% and Δ- 0.6%.

Figure 5- Darcy friction factor versus generalised Reynolds number. X Water, O Tylose 0.4%, Δ Tylose 0.5% and s Tylose 0.6%.

Figure 6- Darcy friction factor versus wall Reynolds number. X Water, O Tylose 0.4%, Δ Tylose 0.5% and s Tylose 0.6%.

Figure 7- Ratio of centreline to bulk velocity versus generalized and wall Reynolds number for X Water, O Tylose 0.4%, Δ Tylose 0.5% and s Tylose 0.6%.

Figure 8a) Axial mean velocity profile in physical coordinates for the 0.4% Tylose solutions. s Re_w= 3030, O Re_w= 4920, + Re_w= 11930, X Re_w= 15400 and Δ Re_w= 19570.

Figure 8b) Axial mean velocity profile in wall coordinates for the 0.4% Tylose solutions. O Re_w= 4920, + Re_w= 11930, X Re_w= 15400 and Δ Re_w= 19570. From Pinho and Whitelaw [19] -Δ-Δ- 0.2% CMC at Re_w= 18260,-x-x- 0.2% CMC at Re_w= 11770,—— 0.1% CMC at Re_w= 16800.

Figure 8c) Axial rms velocity profile in physical coordinates for the 0.4% Tylose solutions. O Re_w= 4920, + Re_w= 11930, X Re_w= 15400 and Δ Re_w= 19570. —— Water Re= 117500. From Pinho and Whitelaw [19] -s- 0.2% CMC at Re_w= 18260,- n - 0.2% CMC at Re_w= 11770, ⊞ 0.1% CMC at Re_w= 16800.

Figure 8d) Radial rms velocity profile in physical coordinates for the 0.4% Tylose solutions. O Re_w= 4920, + Re_w= 11930, X Re_w= 15400 and Δ Re_w= 19570. —— Water Re= 117500. From Pinho and Whitelaw [19] -s- 0.2% CMC at Re_w= 18260,- n - 0.2% CMC at Re_w= 11770, ⊞ 0.1% CMC at Re_w= 16800.

Figure 8e) Azimuthal rms velocity profile in physical coordinates for the 0.4% Tylose solutions. O Re_w= 4920, + Re_w= 11930, X Re_w= 15400 and Δ Re_w= 19570. ── Water Re= 117500. From Pinho and Whitelaw [19] -s- 0.2% CMC at Re_w= 18260,- n - 0.2% CMC at Re_w= 11770, ⊞ 0.1% CMC at Re_w= 16800.

Figure 9a) Axial mean velocity profile in physical coordinates for the 0.6% Tylose solutions. O Re_w= 2160, + Re_w= 4860, X Re_w= 7100 and Δ Re_w= 7950.

Figure 9b) Axial mean velocity profile in wall coordinates for the 0.6% Tylose solutions. O Re_w= 2160, + Re_w= 4860, X Re_w= 7100 and Δ Re_w= 7950.

Figure 9c) Axial rms velocity profile in wall coordinates for the 0.6% Tylose solutions. + Re_w= 4860, X Re_w= 7100 and Δ Re_w= 7950.

Figure 9d) Radial rms velocity profile in wall coordinates for the 0.6% Tylose solutions. Δ Re_w= 7950.

Figure 9e) Azimuthal rms velocity profile in wall coordinates for the 0.6% Tylose solutions. Δ Re_w= 7950.

Figure 10 a) Law of the wall for the Tylose and 0.2% CMC solution of Pinho and Whitelaw [19] at Re_w≈ 12,000. Δ 0.4% Tyl. Re= 11930; X 0.5% Tyl. Re= 13260, + 0.6% Tyl. Re= 7950. - - - 0.2%CMC Re= 11770.

Figure 10 b) Rms of the axial velocity component for the Tylose and 0.2% CMC solution of Pinho and Whitelaw [19] at Re_w≈ 12,000. Δ 0.4% Tyl. Re= 11930; X 0.5% Tyl. Re= 13260, + 0.6% Tyl. Re= 7950. - - - 0.2%CMC Re= 11770,── water Re= 31000.

Figure 10 c) Rms of the radial velocity component for the Tylose and 0.2% CMC solution of Pinho and Whitelaw [19] at Re_w≈ 12,000. Δ 0.4% Tyl. Re= 11930; X 0.5% Tyl. Re= 13260, + 0.6% Tyl. Re= 7950. - - - 0.2%CMC Re= 11770,── water Re= 31000.

Figure 10 d) Rms of the azimuthal velocity component for the Tylose and 0.2% CMC solution of Pinho and Whitelaw [19] at Re_w≈ 12,000. Δ 0.4% Tyl. Re= 11930; X 0.5% Tyl. Re= 13260, + 0.6% Tyl. Re= 7950. - - - 0.2%CMC Re= 11770,── water Re= 31000.